

Exploiting Protein Conformational Change to Optimize Adenosine-Derived Inhibitors of HSP70

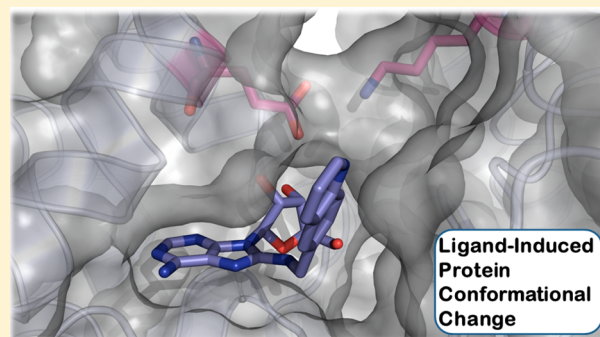
Matthew D. Cheeseman,[†] Isaac M. Westwood,^{†,‡} Olivier Barbeau,[†] Martin Rowlands,[†] Sarah Dobson,^{†,‡} Alan M. Jones,[†] Fiona Jeganathan,[†] Rosemary Burke,[†] Nadia Kadi,[†] Paul Workman,[†] Ian Collins,[†] Rob L. M. van Montfort,^{†,‡} and Keith Jones^{*,†}

[†]Cancer Research UK Cancer Therapeutics Unit, The Institute of Cancer Research, London SW7 3RP, U.K.

[‡]Division of Structural Biology, The Institute of Cancer Research, London SW7 3RP, U.K.

S Supporting Information

ABSTRACT: HSP70 is a molecular chaperone and a key component of the heat-shock response. Because of its proposed importance in oncology, this protein has become a popular target for drug discovery, efforts which have as yet brought little success. This study demonstrates that adenosine-derived HSP70 inhibitors potentially bind to the protein with a novel mechanism of action, the stabilization by desolvation of an intramolecular salt-bridge which induces a conformational change in the protein, leading to high affinity ligands. We also demonstrate that through the application of this mechanism, adenosine-derived HSP70 inhibitors can be optimized in a rational manner.



INTRODUCTION

Heat-shock proteins are a highly conserved family of molecular chaperones that facilitate the folding, stability, and cellular localization of their substrate proteins.¹ Up-regulation of the pathways associated with the heat-shock response has been implicated in a number of disease areas, including cancer.² Recent focus has been on the inhibition of the molecular chaperone heat-shock protein 90 (HSP90) using adenosine triphosphate (ATP) competitive inhibitors, an approach that has resulted in considerable success as several compounds have now entered clinical trials.³ The heat-shock protein 70 (HSP70) family of molecular chaperones represents another potential target for small-molecule mediated antagonism of the heat-shock response pathway. The HSP70 isoform, heat-shock cognate 70 (HSC70), is ubiquitously expressed in tissues, while the inducible isoform, heat-shock protein 72 (HSP72), is largely expressed in response to stress, including treatment with HSP90 inhibitors, and aids cell survival through inhibition of several apoptotic pathways.⁴ We have previously shown that dual knockdown of these two HSP70 isoforms in human colon and ovarian tumor cell lines results in apoptosis, which was in contrast with nontumorigenic cell lines where apoptosis was not observed, indicating a potential therapeutic window for HSP70 inhibitors.⁵

To execute their refolding activity, the HSP70 proteins utilize the hydrolysis of ATP to adenosine diphosphate (ADP) and inorganic phosphate (ADP/P_i) in a complex catalytic cycle involving a number of protein conformational changes and through a process which is tightly regulated by various cochaperones such as the heat-shock protein 40 (HSP40)

proteins and the nucleotide exchange factor BAG family molecular chaperone regulator 1 (BAG1) protein.⁶ While this complexity presents numerous opportunities to antagonize the refolding activity of HSP70, the clearest strategy remains ATP-competitive binding of inhibitors to the conserved nucleotide-binding domain of the protein. Unfortunately, this approach has proven particularly challenging. There remains only one published chemotype which displays ATP-competitive sub-micromolar inhibition of HSP70 and has been shown to be effective in cellular assays, a chemotype derived from adenosine (Figure 1).^{7–10}

The ATPase domain of HSP70 is a member of the actin ATPase family of proteins, a target class which has delivered very little success in the discovery of high affinity ligands.¹¹ A recent study¹² to assess the potential of the HSP70-ATP binding site for antagonism with small molecules using SiteMap¹³ described the target as “difficult”,¹⁴ while a separate analysis using a fragment-based screening approach returned a very low hit rate (0.4%),¹² a result generally associated with low ligandability.¹⁵ Several studies into the biochemical mechanism of HSP70 refolding activity and ATP hydrolysis have demonstrated that the ATP binding site of HSP70 in solution is highly flexible in nature, undergoing numerous conformational changes.¹⁶

With the challenge of finding ATP-competitive hit matter against HSP70 hindering the potential development of inhibitors for this important target, we sought to investigate

Received: December 24, 2015

Published: April 27, 2016

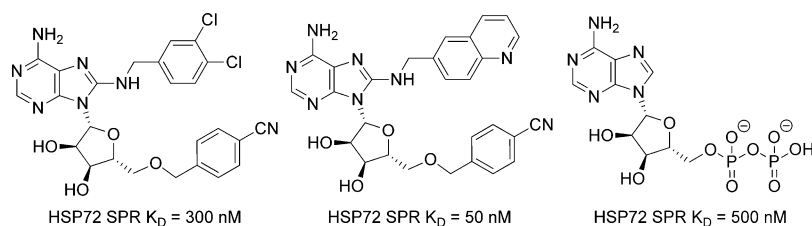


Figure 1. Adenosine-derived ATP-competitive inhibitors of HSP70. The affinity of three known HSP70 inhibitors derived from adenosine and measured by SPR, see ref 7 for details.

the binding mechanism of adenosine-derived ligands to the ATP site of HSP70. The aim was to improve our understanding of how high affinity ligands bind to this region of the protein so that this knowledge could be applied to future inhibitor design.

RESULTS AND DISCUSSION

Development of Toyocamycin Derived Ligands. The slow turnover of ATP by HSP70, and the potent product inhibition by ADP/P_i,¹⁷ means that using functional assays is a challenge for the characterization of HSP70 ligand binding. Therefore, we focused on surface plasmon resonance (SPR) as a biophysical method to assess the affinity of ligands. Unfortunately, full-length human HSP72 gave poor SPR data in our hands, displaying erratic and difficult to interpret sensorgrams. Therefore, the nucleotide-binding domain (NBD) of human HSC70 (HSC70-NBD residues 1–381)¹⁸ was used in all SPR experiments. Adenosine **1** is a relatively weak ligand for HSC70-NBD, displaying a $pK_D = 3.95 \pm 0.01$ ($K_D = 110 \mu\text{M}$, $n = 3$),¹⁹ when measured by SPR, but we decided to use this compound as a starting point for our investigations into the binding mechanisms of this chemotype to the HSP70 proteins. We began by analyzing the importance of the ribose motif to the binding affinity of adenosine **1**. Removing either the 2'- or 3'-hydroxyl groups²⁰ from the sugar motif or changing their relative and absolute stereochemistry resulted in no measurable binding being observed with concentrations up to 1 mM (see [Supporting Information](#)). Removal of either the 6-amino group or the 3-nitrogen of the adenine ring also resulted in the loss of all measurable affinity. These results demonstrate the importance of the ribose motif and the adenine amino-pyrimidine motif to binding of adenosine-derived ligands to the hydrophilic region of the protein. In contrast, removal of the 5'-hydroxyl was well tolerated, as compound **2** retained its affinity in the SPR assay with a $pK_D = 3.88 \pm 0.02$ ($K_D = 130 \mu\text{M}$, $n = 3$) ([Figure 2](#) and [Supporting Information Table 1](#)).²¹

It has previously been shown by Massey et al. that addition of a primary or secondary amine to the 8-position of adenosine resulted in a significant increase in affinity for these ligands.⁷ In our hands, 8-aminoadenosine **3** gave a $pK_D = 5.16 \pm 0.01$ ($K_D = 7.0 \mu\text{M}$, $n = 3$), a 16-fold increase in affinity when compared

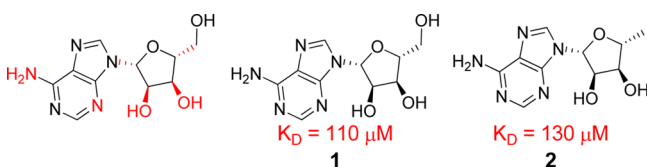


Figure 2. 5'-Hydroxyl has little effect on affinity. The heteroatoms and stereochemistry highlighted in red are important for affinity to HSP70 and could not be replaced by hydrogen or CH or the stereochemistry changed.

to adenosine **1**. We decided to investigate this substituent in order to better understand its role in the improved affinity of these compounds ([Table 1](#)).

Table 1. 8- and 5'-Substituted Adenosine Based HSP70 Ligands

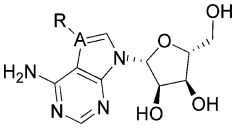
Entry	Compd.	R ¹	R ²	$pK_D \pm \text{SEM}^a$	$K_D (\mu\text{M})^b$
1	3	NH_2	OH	5.16 ± 0.01	7.0
2	4	$\text{N}^{\text{H}}\text{Me}$	OH	4.77 ± 0.02	17
3	5	$\text{N}^{\text{Me}}\text{Me}$	OH	< 3.00	> 1000
4	6	O^{Me}	OH	< 3.00	> 1000
5	7	$\text{N}^{\text{H}}\text{Me}$	H	4.56 ± 0.01	27

^aAll results are quoted as the geometric mean \pm standard error of the mean (SEM) of three independent experiments unless otherwise stated, $pK_D = -\log_{10}(K_D(\mu\text{M}) \times 10^{-6})$. ^bAll values are quoted to 2 significant figures.

Methyl substitution on the 8-amino group (entry 2) gave ligand **4** and resulted in a 2.5-fold drop in affinity,²² while dimethyl analogue **5** (entry 3) displayed a K_D greater than 1 mM. Replacement of the 8-amino substituent with a methoxy group to give **6** (entry 4) also resulted in a complete loss of activity. This dramatic effect on binding suggested that one of the hydrogens of the 8-amino group was involved in hydrogen bonding. To assess whether an intramolecular hydrogen bond to the 5'-hydroxyl was important for affinity, we removed this group to give **7** (entry 5). However, only a 1.6-fold drop in affinity was observed with analogue **7** when compared with 8-*N*-methylaminoadenosine **4** (entry 2). These results suggest that an intramolecular hydrogen bond between the 8-amino substituent and the 5'-hydroxyl group cannot rationalize the increased affinity observed with the 8-aminoadenosine series.²³ We speculated that the role of the 8-amino substituent as a hydrogen bond donor is through interactions with the cyclic ribose oxygen to stabilize a gauche conformation of adenosine, which facilitates binding by reducing the energy barrier to the initial binding event.²⁴

Finally, we sought to investigate the role of the imidazole ring of adenosine to the binding of these ligands to HSP70 (Table 2).

Table 2. Natural Product Nucleoside Derived HSP70 Ligands



Entry	Compd.	Name ^a	R	A	pK _D ±SEM ^b	K _D (μM) ^c
1	1	Adenosine	H	N	3.95±0.01	110
2	8	Tubercidin	H	C	4.55±0.26	28
3	9	Toyocamycin	C≡N	C	4.04±0.01	90
4	10	Sangivamycin	H ₂ N	C	5.49±0.02	3.3

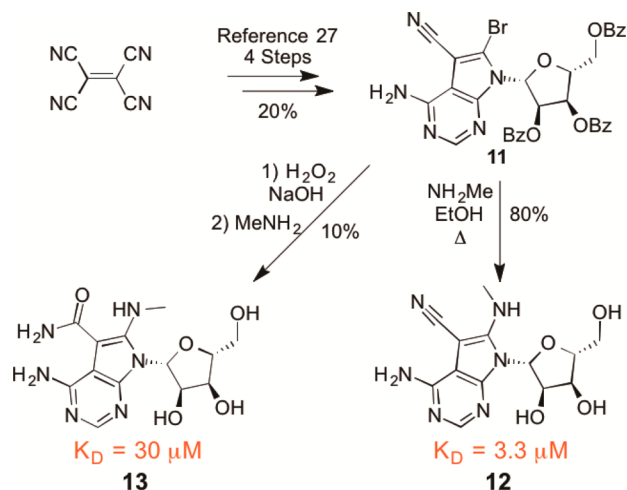
^aAll compounds were purchased from the relevant commercial suppliers and used without further purification. ^bAll results are quoted as the geometric mean ± SEM of three independent experiments unless otherwise stated, pK_D = -log₁₀(K_D(μM) × 10⁻⁶). ^cAll values are quoted to 2 significant figures.

We screened three commercially available bacterial natural products, all based on the replacement of the purine of adenosine with a pyrolopyrimidine scaffold, exchanging the nitrogen at the 7-position²⁵ with carbon.²⁶ Comparing this change in scaffold to adenosine **1** (entry 1): the more lipophilic derivative tubercidin **8** (entry 2) displayed a 4-fold improvement in affinity, substitution at the 7-position was well tolerated, with the nitrile derivative toyocamycin **9** (entry 3) displaying comparable affinity to adenosine **1**, and the primary amide derivative sangivamycin **10** (entry 4) gave a 35-fold increase in affinity at 3.3 μM.

With knowledge of the increased affinity observed with the pyrolopyrimidine scaffold in hand, we planned to combine the scaffold hop with the improved affinity previously described for 8-amino substitution of the adenosine scaffold. 8-Amino substitution of tubercidin proved synthetically intractable due to the absence of an electron-withdrawing group at the 7-position, making aromatic substitution at the 8-position challenging. Therefore, we focused our efforts on the synthesis of 8-aminotoyocamycin **12** and 8-aminosangivamycin **13** (Scheme 1).

Tribenzoyl intermediate **11** was prepared in four steps and 20% yield using a previously described procedure.²⁷ Despite repeated attempts, we were unable to introduce an ammonia equivalent to the 8-position. However, we were successful using methylamine as a nucleophile to give 8-*N*-methylaminotoyocamycin **12**, which underwent in situ deprotection of the benzoyl groups under the reaction conditions. Treatment of intermediate **11** with basic hydrogen peroxide resulted in hydrolysis of the nitrile group, and subsequent addition of methylamine gave 8-*N*-methylaminosangivamycin **13** in low yield and moderate purity.²⁸ 8-*N*-Methylaminotoyocamycin **12** gave a pK_D = 5.47 ± 0.02 (K_D = 3.3 μM, n = 3) against HSC70-NBD. This result represented a 27-fold improvement in activity compared to toyocamycin **9** (Table 2, entry 1) and a 5-fold increase in affinity when compared to the corresponding 8-*N*-methyladenosine **12** (Table 1, entry 2). In contrast, 8-*N*-

Scheme 1. Natural Product Derived Ligands of HSP70



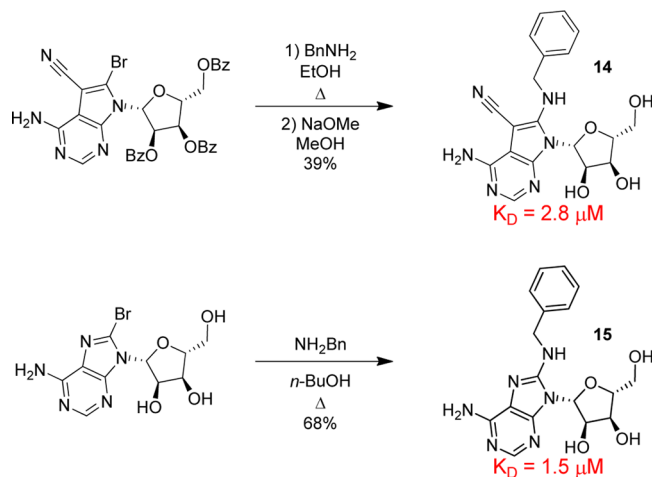
methylsangivamycin **13** gave a pK_D = 4.52 (K_D = 30 μM, n = 1),²⁹ which is a 7-fold drop in affinity compared to sangivamycin **10** (Table 2, entry 3). We rationalized this structure–activity relationship (SAR) through the potential effect of the 7-substituent on the hydrogen bonding ability of the key 8-*N*-methylamino group. The primary amide substituent of **13** can form an intramolecular hydrogen bond with the 8-*N*-methylamino group to give a resonance stabilized six-membered intramolecular hydrogen bond,³⁰ which would mask the hydrogen bond donor effect of the 8-*N*-methylamino substituent and block the binding of this ligand.

To develop the toyocamycin scaffold further, we sought to introduce a benzylic substituent to the 8-position amine. Previously, Massey et al. have shown that *N*-benzyl substitution at the 8-amino position could improve the affinity of adenosine derived inhibitors of HSP70 (Figure 1).⁷ Because our toyocamycin derived scaffold **12** had displayed a 5-fold improvement in affinity compared to the corresponding adenosine scaffold **4**, we hypothesized that addition of an 8-*N*-benzyl substituent to toyocamycin would result in an improved chemotype for HSP70 inhibition. 8-*N*-Benzyltoyocamycin **14** was prepared via a similar method to **12** using benzylamine as a nucleophile. For comparison, 8-*N*-Benzyladenosine **15** was prepared in one step via a literature procedure from commercially available 8-bromoadenosine (Scheme 2).³¹

8-*N*-Benzyladenosine derivative **15** gave a pK_D = 5.84 ± 0.02 (K_D = 1.5 μM, n = 3), representing a 12-fold improvement in binding affinity compared to the 8-*N*-methyladenosine analogue **4** (Table 1, entry 2); however, the 8-*N*-benzyltoyocamycin analogue **14** gave a pK_D = 5.56 ± 0.02 (K_D = 2.8 μM, n = 3), representing little change in affinity compared to 8-*N*-methyltoyocamycin derivative **12** despite the increase in molecular weight and lipophilicity. Even though toyocamycin **9** was apparently an improved scaffold, when compared to adenosine, for the inhibition of HSP70, we had been unable to develop the compounds beyond a micromolar affinity ligand. We believed that improving our understanding of the complex SAR surrounding the nucleoside core and lipophilic 8-*N*-benzyl substituent through analysis of ligand/HSP70 co-crystal structures would be crucial to the discovery and development of small-molecule inhibitors of HSP70.

HSP70 Conformations. In 1995, kinetic studies by McKay and Ha using changes in tryptophan fluorescence indicated that the HSP70 isoform, HSC70, undergoes a number of conforma-

Scheme 2. 8-N-Benzyl Derivatives of Adenosine Analogues



tional changes during its catalytic cycle.³² The energy released from ATP hydrolysis drives subsequent conformational changes in the substrate binding domain, allowing HSP70 to carry out its refolding function on client proteins. However, McKay and Ha discovered that ATP and ADP have two distinct binding mechanisms. While ADP binds and then dissociates in an apparent single-step mechanism with slow-off kinetics, the binding of ATP is a two-step process, requiring an additional conformational change of the nucleotide-binding domain prior to ATP hydrolysis. Because it had been demonstrated that the two nucleotide substrates of HSP70 can jump between binding mechanisms, we hypothesized that the complexity surrounding the apparent SAR of the nucleoside derived HSP70 inhibitors was due to a change in mechanism between a one-step and an induced conformational change two-step mechanism, even if kinetically this would be difficult to observe.³³

To investigate whether a two-step binding model is consistent with the observed nucleoside SAR, we decided to probe HSP70 ligand binding by X-ray crystallography. There is currently no crystal structure of full-length human HSP70; therefore, we focused our crystallography efforts on the NBD of the human HSP70 isoform HSP72 (HSP72-NBD).

In our hands, ADP **16** gave an affinity of $pK_D = 6.49$ ($K_D = 0.32 \mu\text{M}$, $n = 1$) when measured by SPR against the HSC70-NBD.³⁴ The co-crystal structure of ADP/P_i bound to the HSP72-NBD has previously been solved^{16a} and analysis of this structure clearly revealed a closed conformation of the protein. The two α -helices flanking the sides of the ATP binding site, closed around the adenosine motif of ADP, forming multiple hydrogen bonds with the ribose and adenine moieties of ADP (Figure 3).

From analysis of this structure, the two phosphate groups of ADP form multiple hydrogen bonds within the phosphate binding region of the HSP72-NBD. It is also clear that the HSP72-NBD would need to undergo a conformational change in order for ADP/P_i to dissociate, resulting in the previously described slow-off kinetics.³² It has been suggested previously that the closed conformation is apparently stabilized by the formation of a solvent exposed salt-bridge between glutamic acid-268 and lysine-56.³⁵ Intrigued by the formation of this intramolecular interaction, we then sought to generate a co-crystal structure with the bacterial natural product sangivamycin **10** ($K_D = 3.3 \mu\text{M}$) (Figure 4).

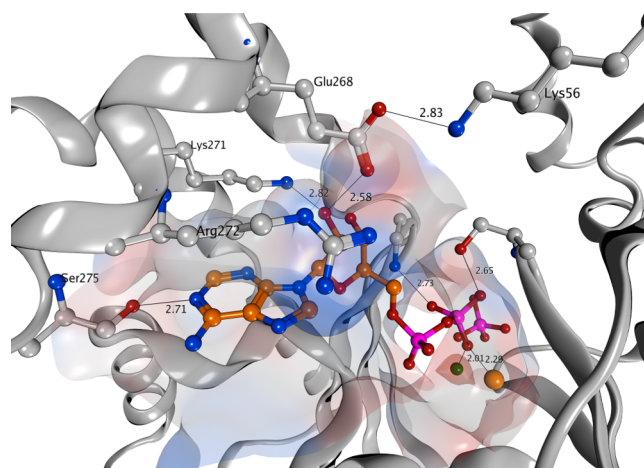


Figure 3. Crystal Structure of ADP/P_i bound to HSP72. PDB 3ATU, important hydrogen bonding interactions, with their distances in Å, and residues are indicated. The key salt-bridge interaction between lysine-56 and glutamic acid-268 was measured at 2.8 Å (2 SF). Orange and turquoise spheres represent sodium and magnesium ions, respectively. Only selected residues are shown and solvent has been omitted for clarity.

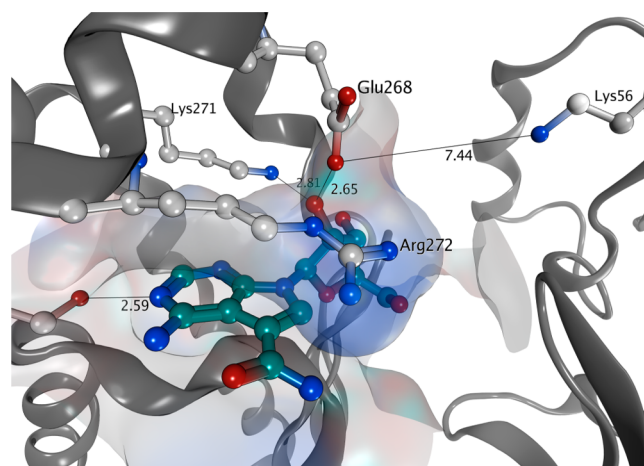


Figure 4. Co-crystal structure of sangivamycin **10** bound to HSP72. PDB 5AQZ, key hydrogen bonding interactions and their distances in Å are indicated. The key salt-bridge interaction between lysine-56 and glutamic acid-268 is absent. Only selected residues are shown and solvent has been omitted for clarity.

The crystal structure of sangivamycin **10** revealed a similar hydrogen bonding framework to the adenosine motif of the ADP/P_i structure (Figure 3). The pyrrolopyrimidine ring interacts with serine-275 and the 2'- and 3'-hydroxyls of the ribose interact with lysine-271. However, in contrast to the ADP/P_i HSP72-NBD structure, sangivamycin **10** co-crystallized in a more open conformation. The two α -helices of the nucleotide binding domain are no longer in close proximity, and the solvent exposed salt-bridge between glutamic acid-268 and lysine-56 is absent. It is this difference in the HSP70-NBD conformation which we hypothesize is an important factor in the complexity of SAR observed for nucleoside-derived inhibitors. The binding of both ADP/P_i and sangivamycin **10** are dominated by the formation of multiple hydrogen bonds to key residues in the nucleoside binding cleft but the crucial difference between the two ligands is their ability to induce and stabilize the closed conformation of the HSP72-NBD. It is this

ligand-driven induced conformational change that leads to high affinity for HSP70. The HSP72-NBD closed conformation observed in the ADP/P_i bound structure is presumably brought about by the interactions of the β -phosphate group with the two glycine-rich loops of the phosphate binding region. We speculated that this conformational change could force water molecules from the nucleotide binding domain cleft, strengthening the many hydrogen bond contacts surrounding the adenosine due to the more hydrophobic environment. The absence of the phosphate groups, and in particular the β -phosphate group, in sangivamycin **10** means there is no induced conformational change so the affinity is only dependent on the multiple hydrogen bonds (Figure 5).

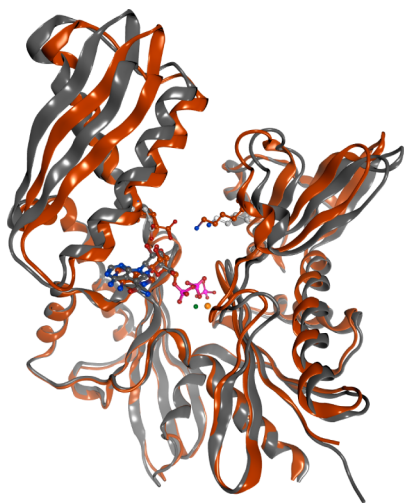
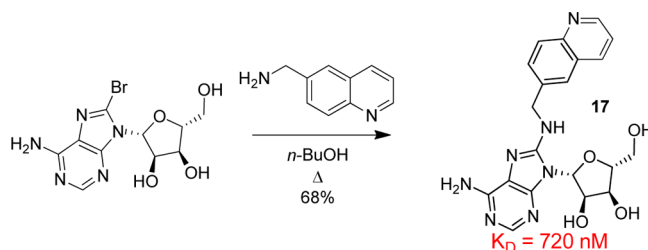


Figure 5. Induced open and induced closed conformations of HSP72. PDB 3ATU and 5AQZ, the copper-colored structure represents the co-crystal structure of ADP/P_i bound to the HSP72-NBD in the induced closed conformation due to interactions of the phosphate groups through hydrogen bonds with the glycine rich loops and stabilized by the salt-bridge. The gray-colored structure represents the co-crystal structure of sangivamycin **10** bound to the HSP72-NBD. The overlay shows sangivamycin **10** bound to a more open NBD conformation, in which the formation of the Glu-Lys salt-bridge is not possible. Only selected residues are shown and solvent has been omitted for clarity.

An Alternative Approach to Inducing the Closed Conformation of HSP70. Mimicking phosphate groups with druglike ligands represents a significant challenge in medicinal chemistry.³⁶ However, if it were possible to induce the closed conformation of the HSP70 nucleotide binding domain via an alternative mechanism, then mimicking the β -phosphate would be unnecessary. Because the solvent exposed salt-bridge between glutamic acid-268 and lysine-56 was the only additional enthalpic intradomain interaction that we observed in the HSP70-NBD closed conformation structure, when compared with the more open sangivamycin **10** structure, we hypothesized that a ligand stabilizing this interaction would stabilize the closed conformation of HSP70, leading to increased affinity. We therefore proposed that the previously described potent 8-*N*-benzyladenosine derived ligands were able induce a conformational change in HSP70 but via a lipophilic mechanism, which would be more amenable to drug discovery. To investigate this hypothesis, we synthesized the known quinoline derived HSP70 inhibitor **17** in one step and 68% yield using our previously described method (Scheme 3).⁷

Scheme 3. Synthesis of Quinoline Adenosine Derivative



Although several 8-*N*-substituted HSP70 inhibitors have been described in the literature,⁷ the 8-*N*-quinoline adenosine derived ligand **17** was chosen because it was reported to be the highest affinity ligand which was only substituted at the 8-position. In our hands, **17** gave a pK_D = 6.14 ± 0.01 (K_D = 0.72 μM, *n* = 3) against HSC70-NBD when measured by SPR, which was consistent with the data reported in the literature.³⁷ 8-*N*-Quinoline aminoadenosine derived ligand **17** was then submitted to our co-crystallization protocol with HSP72-NBD (Figure 6).

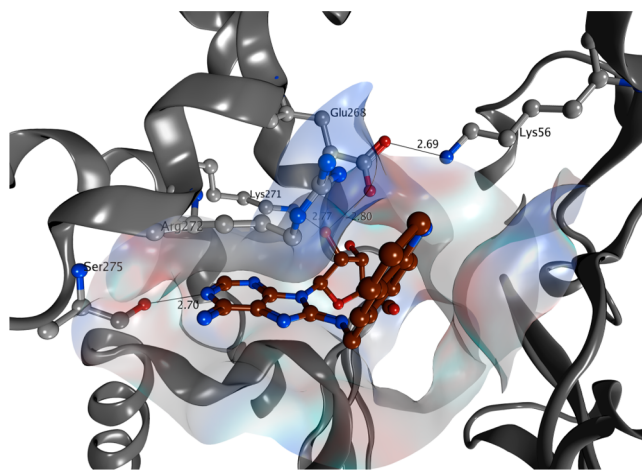


Figure 6. Co-crystallization of 8-*N*-quinoline aminoadenosine derived ligand **17** bound to HSP72. PDB 5AR0, the HSP72 structure clearly demonstrates the formation the key salt-bridge when co-crystallized with 8-*N*-quinolineadenosine **17**. Important hydrogen bonding interactions are indicated with their distances in Å. Only selected residues are shown and solvent has been omitted for clarity.

Co-crystallization of **17** with the HSP72-NBD showed the NBD in a closed conformation (Figure 5), nearly identical to the conformation of the HSP72-NBD in the ADP/P_i bound structures (Figure 6). To our knowledge, this is the first example of a co-crystal structure demonstrating a non-nucleotide ligand binding to the closed conformation of HSP70. The similarity of the respective HSP72 conformations is consistent with a potential role of the induced conformational change in enhancing the affinity of the 8-*N*-benzyl nucleoside derived HSP70 ligands. However, the mechanism by which the inhibitor induced conformational change occurs must be distinctly different from the mechanism of NBD closure upon nucleotide binding because the quinoline moiety of **17** forms no interactions within the phosphate binding region.

To rationalize the induced conformational change observed with **17**, we further analyzed the closed structure of HSP72-NBD to identify the key binding interactions. 8-*N*-Quinoline adenosine **17** displays a similar hydrogen bonding network with

the same key residues observed in both ADP/P_i and sangivamycin **10**, with an additional solvent exposed water molecule bound to the quinoline nitrogen. However, in contrast with the more open conformation observed in the HSP72-NBD sangivamycin **10** complex, the key salt-bridge between glutamic acid-268 and lysine-56, which is present in the nucleotide-bound HSP70-NBD structures, is clearly formed in the **17**-bound HSP72-NBD structure (Figure 5). In the ADP/P_i/HSC70-NBD co-crystal structure, the salt-bridge is solvent exposed, weakening its effect (Figure 7).³⁸ By contrast,

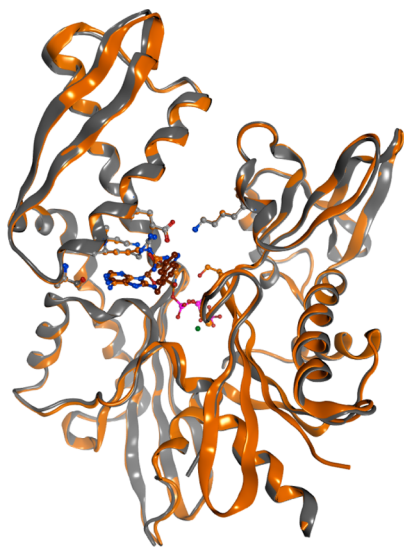


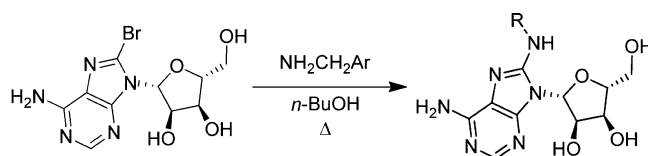
Figure 7. Overlay of ADP/P_i and 8-*N*-quinoline adenosine **17** co-crystal structures with HSP72. PDB 3ATU and SAR0, overlay of the ADP/P_i-HSP72 co-crystal structure (copper) and the 8-*N*-quinoline adenosine **17**-HSP72 co-crystal structure (gray). Only selected residues are shown and solvent has been omitted for clarity.

in the **17**-bound HSP72-NBD co-crystal structure, the quinoline moiety is able to form a π -stack with arginine-272, although this interaction is solvent exposed so is only likely to be weak;³⁹ the result is to place the quinoline group directly in front of the salt-bridge. Because the quinoline is highly lipophilic, this creates a more lipophilic environment surrounding the salt-bridge, protecting it from water and strengthening the interaction, which leads to increased affinity for 8-*N*-benzyl aminonucleoside derived ligands.⁴⁰ We propose the binding mechanism of these ligands to HSP70 is analogous to a “door and latch”. The initial binding event is similar for all nucleoside derived ligands of HSP70 and is dominated by hydrogen bonds to serine-275 and lysine-271. The nucleotide binding domain is then able to close around the ligand but for this process to be favorable, when balanced by the entropy cost of restricting the conformational freedom of the protein, it must be stabilized by the ligand. ADP can achieve this through interactions with the phosphate binding region, while quinoline ligand **17** stabilizes the key salt-bridge through hydrophobic desolvation. Sangivamycin **10** has neither of these substituents so predominately binds to the open conformation.

Optimizing the 8-Position. To test this hypothesis, and to generate more active ligands of HSP70 for further development, we synthesized a series of 8-*N*-benzylaminonucleoside analogues using our previously described method (Table 3).

The 8-*N*-benzyl derivative **15**, as shown previously, gave a $pK_D = 5.84 \pm 0.02$ ($K_D = 1.4 \mu\text{M}$, $n = 3$) when measured by

Table 3. 8-Position Optimization of Adenosine Derived HSP70 Ligands



Entry	Compd.	R	$pK_D \pm \text{SEM}^a$	K_D (μM) ^b
1	17		6.14 ± 0.01	0.72
2	15		5.84 ± 0.02	1.4
3	18		6.55 ± 0.01^c	0.28
4	19		6.34 ± 0.01	0.46
5	20		6.53 ± 0.01	0.30
6	21		5.45 ± 0.01	3.5

^aAll results are quoted as the geometric mean \pm SEM of three independent experiments unless otherwise stated, $pK_D = -\log_{10}(K_D(\mu\text{M}) \times 10^{-6})$. ^bAll values are quoted to 2 significant figures. ^cThe geometric mean of $n = 9$ experiments.

SPR against HSC70-NBD. The weaker activity observed with the benzyl group **15** compared to quinoline **17** we rationalized was due to its less efficient desolvation of the glutamic acid/lysine salt bridge by the smaller lipophilic group. Therefore, we decided to add a number of lipophilic substituents to assess whether we could improve the desolvation effect, promote the induced closed conformation, and improve the affinity of the ligands. *para*-Chloro-substitution gave adenosine derivative **18** (entry 3) with a $pK_D = 6.55 \pm 0.01$ ($K_D = 0.28 \mu\text{M}$, $n = 9$), a 5-fold improvement in affinity compared to compound **15** and a 60-fold improvement compared to 8-*N*-methylaminoadenosine **4** (Table 1, entry 2). Although the kinetics of these ligands binding to HSP70 were at the limit of what could be accurately measured by SPR, analysis of the off-rate did reveal that the quinoline ligand **17** and the *para*-chlorobenzyl derivative **18** possessed measurably slow off-rates compared to sangivamycin **10**, whose half-life was too short to be observed with this technique (see Supporting Information for details).⁴¹ Similar improvements were also observed for the *para*-fluoro derivative **19** (entry 4, $pK_D = 6.34 \pm 0.01$, $K_D = 0.46 \mu\text{M}$, $n = 3$) and *para*-methyl derivative **20** (entry 5, $pK_D = 6.53 \pm 0.01$, $K_D = 0.30 \mu\text{M}$, $n = 3$). Because the crystal structure of this ligand class shows that the benzylic moiety resides in the cleft formed by the two α -helices in the nucleotide binding domain of HSP70, it is unlikely that the *para*-lipophilic substituents interact with HSP70 via a lipophilic pocket, as the group is essentially solvent exposed. This effect could not be explained by an increase in the overall lipophilicity of the ligand to exploit the nonspecific hydrophobic effect because dichlorobenzyl derivative **21** (entry 6, $pK_D = 5.45 \pm 0.01$, $K_D = 3.5 \mu\text{M}$, $n = 3$) displayed a significant drop in affinity.

CONCLUSIONS

The ATP binding site of HSP70 is a challenging region of the protein to target with small molecules due to its hydrophilic nature and high flexibility. To target the nucleotide binding domain it is important to understand the conformational changes that this region of the protein undergoes. Using protein/ligand X-ray crystallography, we have demonstrated

that non-nucleotide ligands of HSP70 can induce conformational changes in the protein and that these changes can play an important role in the binding of HSP70 inhibitors. In solution, kinetic studies suggest that this protein undergoes a number of conformational changes of not just the nucleotide binding domain but also the substrate-binding domain.³² Also, interactions between these two domains and the role of cochaperones in these conformational changes have yet to be addressed. Better understanding of the flexibility of HSP70 and its effect on the affinity of ligands will contribute to better assay design and more efficient inhibitor optimization.

EXPERIMENTAL SECTION

Experimental Procedures (Chemistry). Unless otherwise stated, reactions were conducted in oven-dried glassware under an atmosphere of nitrogen using anhydrous solvents. All commercially obtained reagents and solvents were used as received. Thin layer chromatography (TLC) was performed on precoated aluminum sheets of silica (60 F254 nm, Merck) and visualized using short-wave UV light. Flash column chromatography was carried out on Merck silica gel 60 (partial size 40–65 μm). ^1H NMR spectra were recorded on Bruker AMX500 (500 MHz) spectrometers using an internal deuterium lock. Chemical shifts are quoted in parts per million (ppm) using the following internal references: CDCl_3 (δH 7.26), MeOD (δH 3.31), and DMSO- d_6 (δH 2.50). Signal multiplicities are recorded as singlet (s), doublet (d), triplet (t), quartet (q), multiplet (m), doublet of doublets (dd), doublet of doublet of doublets (ddd), apparent triplet (app t) broad (br), or obscured multiplet (obs m). Coupling constants, J , are measured to the nearest 0.1 Hz. ^{13}C NMR spectra were recorded on Bruker AMX500 spectrometers at 126 MHz using an internal deuterium lock. Chemical shifts are quoted to 0.01 ppm, unless greater accuracy was required, using the following internal references: CDCl_3 (δC 77.0), MeOD (δC 49.0), and DMSO- d_6 (δC 39.5). High resolution mass spectra were recorded on an Agilent 1200 series HPLC and diode array detector coupled to a 6210 time-of-flight mass spectrometer with dual multimode APCI/ESI source. Analytical separation was carried out on a Merck Purospher STAR RP-18, 30 mm \times 4 mm column using a flow rate of 1.5 mL/min in a 4 min gradient elution, UV detection was at 254 nm. All compounds were >95% purity by HPLC analysis unless otherwise stated.

(2R,3R,4S,5R)-2-(6-Amino-8-(methylamino)-9H-purin-9-yl)-5-(hydroxymethyl)tetrahydrofuran-3,4-diol 4. To a solution of 8-bromoadenosine (0.051 g, 0.15 mmol) in EtOH (1.5 mL) was added methylamine solution (33% solution in EtOH, 0.25 mL, 3.0 mmol), and the mixture was heated to 80 °C for ~12 h. After this time, the mixture was cooled to room temperature and the solvent removed under reduced pressure. The resulting residue was purified by silica gel chromatography eluting with 2 M MeOH/ NH_3 :EtOAc (8:2) to give the desired compound as a white solid (0.031 g 71%); δH (500 MHz, DMSO- d_6) 7.90 (s, 1H), 6.95 (d, J = 4.8 Hz, 1H), 6.57 (s, 2H), 5.92 (dd, J = 6.0, 4.0 Hz, 1H), 5.86 (d, J = 7.3 Hz, 1H), 5.26 (d, J = 6.7 Hz, 1H), 5.16 (d, J = 4.0 Hz, 1H), 4.68 (td, J = 7.0, 5.3 Hz, 1H), 4.12 (ddd, J = 5.6, 4.1, 2.1 Hz, 1H), 3.97 (d, J = 2.3 Hz, 1H), 3.70–3.58 (m, 2H), 2.89 (d, J = 4.5 Hz, 3H); δC (126 MHz, DMSO- d_6) 152.86, 152.52, 150.28, 148.89, 117.64, 86.99, 86.13, 71.42, 71.20, 62.15, 29.59. HRMS (ESI) $\text{C}_{11}\text{H}_{17}\text{N}_6\text{O}_4$ ($\text{M} + \text{H}^+$) requires 297.1306, found 297.1299.

(2R,3R,4S,5R)-2-(6-Amino-8-(dimethylamino)-9H-purin-9-yl)-5-(hydroxymethyl)tetrahydrofuran-3,4-diol 5. To a solution of 8-bromoadenosine (0.064 g, 0.19 mmol) in EtOH (1.9 mL) was added dimethylamine (40% solution in water, 0.42 mL, 3.70 mmol), and the mixture was heated to 80 °C for ~12 h. After this time, the mixture was cooled to room temperature and the solvent removed under reduced pressure. The resulting residue was purified by silica gel chromatography eluting with 2 M MeOH/ NH_3 :EtOAc (9:1) to give the desired product as a white solid (0.027 g, 47%); δH (500 MHz, MeOH) 8.05 (d, J = 1.1 Hz, 1H), 5.91 (d, J = 7.5 Hz, 1H), 5.16 (dd, J = 7.5, 5.3 Hz, 1H), 4.36 (dd, J = 5.2, 1.4 Hz, 1H), 4.14 (d, J = 1.9 Hz, 1H), 3.86 (dd, J = 12.6, 2.3 Hz, 1H), 3.73 (dd, J = 12.6, 2.7 Hz, 1H),

3.03 (s, 6H); δC (126 MHz, MeOD) 157.19, 153.92, 149.92, 149.22, 116.86, 89.06, 86.97, 71.96, 71.79, 62.86, 41.89. HRMS (ESI) $\text{C}_{12}\text{H}_{19}\text{N}_6\text{O}_4$ ($\text{M} + \text{H}^+$) requires 311.1462, found 311.1464.

(2R,3R,4S,5R)-2-(6-Amino-8-methoxy-9H-purin-9-yl)-5-(hydroxymethyl)tetrahydrofuran-3,4-diol 6. To a solution of 8-bromoadenosine (0.11 g, 0.33 mmol) in MeOH (4 mL) was added NaOMe (0.18 g, 3.3 mmol), and the mixture was stirred at room temperature for ~12 h. After this time, the solvent was removed under reduced pressure and the resulting residue was purified by silica gel chromatography eluting with 2 M MeOH/ NH_3 :EtOAc (9:1) to give the desired product as a yellow oil (0.025 g, 26%). δH (500 MHz, MeOD), 8.06 (s, 1H), 5.91 (d, J = 7.1 Hz, 1H), 4.93 (dd, J = 7.0, 5.2 Hz, 1H), 4.33 (dd, J = 5.2, 2.0 Hz, 1H), 4.21 (s, 3H), 4.16–4.09 (m, 1H), 3.86 (dd, J = 12.6, 2.5 Hz, 1H), 3.71 (dd, J = 12.6, 2.9 Hz, 1H); δC (126 MHz, MeOD) 155.19, 154.01, 150.10, 148.34, 115.35, 87.65, 86.82, 72.43, 71.55, 62.62, 56.69. HRMS (ESI) $\text{C}_{11}\text{H}_{16}\text{N}_5\text{O}_5$ ($\text{M} + \text{H}^+$) requires 298.1146, found 298.1152.

(2R,3R,4S,5R)-2-(6-Amino-8-(methylamino)-9H-purin-9-yl)-5-methyltetrahydrofuran-3,4-diol 7. To a solution of 5'-deoxyadenosine (0.024 g, 0.096 mmol) in dioxane (0.48 mL) and water (0.48 mL) was added KH_2PO_4 (0.065 g, 0.29 mmol) and bromine (0.023 g, 0.14 mmol) as a solution in water (0.50 mL), and the mixture was stirred for 15 min. The mixture was then quenched with sodium thiosulfate solution (5.0 mL), extracted with EtOAc, dried (MgSO_4), and the solvent removed under reduced pressure. The resulting residue was used in the next step without further purification.

The product from the previous step (0.032 g, 0.097 mmol) was dissolved in 2 M MeNH₂ in EtOH (1.9 mL), and the mixture was heated to 70 °C for ~12 h. After this time, the mixture was cooled to room temperature and the solvent removed under reduced pressure. The resulting residue was purified by silica gel chromatography eluting with 2 M MeOH/ NH_3 :EtOAc (1:9) to give the desired product as a white solid (0.009 g, 33% over two steps); δH (500 MHz, DMSO- d_6) 7.90 (s, 1H), 6.75 (q, J = 4.5 Hz, 1H), 6.45 (s, 2H), 5.58 (d, J = 4.2 Hz, 1H), 5.23 (d, J = 5.0 Hz, 1H), 5.09 (q, J = 5.0 Hz, 1H), 4.99 (d, J = 5.7 Hz, 1H), 4.14–4.04 (m, 1H), 3.83 (app p, J = 6.2 Hz, 1H), 2.88 (d, J = 4.5 Hz, 3H), 1.24 (d, J = 6.3 Hz, 3H); δC (126 MHz, DMSO- d_6) 152.97, 152.91, 150.19, 149.12, 117.95, 88.07, 79.10, 74.87, 71.05, 29.73, 18.96. HRMS (ESI) $\text{C}_{11}\text{H}_{17}\text{N}_6\text{O}_3$ ($\text{M} + \text{H}^+$) requires 281.1357, found 281.1354.

(2R,3R,4R,5R)-2-(4-Amino-6-bromo-5-cyano-7H-pyrrolo[2,3-d]pyrimidin-7-yl)-5-((benzoyloxy)methyl)tetrahydrofuran-3,4-diyl Dibenzate 11. Prepared via a previously described procedure in four steps and 20% overall yield. The spectroscopic data matched that previously described.⁴²

4-Amino-7-((2R,3R,4S,5R)-3,4-dihydroxy-5-(hydroxymethyl)tetrahydrofuran-2-yl)-6-(methylamino)-7H-pyrrolo[2,3-d]pyrimidine-5-carbonitrile 12. (2R,3R,4R,5R)-2-(4-Amino-6-bromo-5-cyano-7H-pyrrolo[2,3-d]pyrimidin-7-yl)-5-((benzoyloxy)methyl)tetrahydrofuran-3,4-diyl dibenzate 11 (120 mg, 0.17 mmol) was dissolved in 2 M methylamine in ethanol (5.0 mL), and the reaction was heated in a microwave reactor at 140 °C for 1 h. After this time, the mixture was cooled to room temperature and the solvent removed under reduced pressure. The resulting residue was purified by silica gel chromatography with the Biotage SP1 purification system (column, 10+ S ; flow rate, 15 mL/min; gradient starting with 100% DCM from 0 to 1 CV then from 100% DCM to 2% NH_4OH /18% MeOH/80% DCM from 1 CV to 21 CV) to give the desired compound as a white solid (0.045 g, 80% yield); δH (500 MHz, MeOD) 3.22 (s, 3H), 3.83–3.84 (m, 2H), 4.14 (q, J = 1.9 Hz, 1H), 4.27 (dd, J = 5.6, 2.0 Hz, 1H), 4.65 (dd, J = 7.6, 5.6 Hz, 1H), 6.29 (d, J = 7.9 Hz, 1H), 8.01 (s, 1H); δC (126 MHz, MeOD) 29.55, 56.92, 61.31, 70.91, 71.19, 86.12, 87.35, 101.19, 118.75, 148.27, 149.87, 151.26, 154.16. HRMS (ESI) $\text{C}_{13}\text{H}_{17}\text{N}_6\text{O}_4$ ($\text{M} + \text{H}^+$) requires 321.1306, found 321.1303.

4-Amino-7-((2R,3R,4S,5R)-3,4-dihydroxy-5-(hydroxymethyl)tetrahydrofuran-2-yl)-6-(methylamino)-7H-pyrrolo[2,3-d]pyrimidine-5-carboxamide 13. To a solution of (2R,3R,4R,5R)-2-(4-amino-6-bromo-5-cyano-7H-pyrrolo[2,3-d]pyrimidin-7-yl)-5-((benzoyloxy)methyl)tetrahydrofuran-3,4-diyl dibenzate 11 (87 mg, 0.13 mmol) in THF (1.0 mL) was added hydrogen peroxide (33%, 1.0 mL) and 1 M NaOH (1.0 mL). The reaction was stirred at room

temperature for ~18 h before 1 M HCl was added until the mixture reached pH 6, when the solvent was removed under reduced pressure. The resulting residue was dissolved in 2 M methylamine in ethanol (5.0 mL), and the reaction was heated to 120 °C in a microwave reactor for 50 min. After this time, the mixture was cooled to room temperature and the solvent removed under reduced pressure. The resulting residue was purified by silica gel chromatography using the Biotage SP1 purification system (column, 10+S; flow rate, 15 mL/min; gradient starting with 100% DCM from 0 to 1 CV then from 100% DCM to 2% NH₄OH/18% MeOH/80% DCM from 1 CV to 21 CV) to give the desired product as a yellow solid (0.009 g, 10% yield); δ H (500 MHz, MeOD) 2.89 (s, 3H), 3.78 (dd, J = 12.2, 1.9 Hz, 1H), 3.86 (dd, J = 12.2, 2.2 Hz, 1H), 4.18 (q, J = 1.7 Hz, 1H), 4.33 (dd, J = 5.5, 1.3 Hz, 1H), 4.85 (m, 1H), 6.12 (d, J = 7.9 Hz, 1H), 8.02 (s, 1H); δ C (126 MHz, MeOD) 35.35, 62.23, 71.62, 72.28, 86.70, 87.49, 98.51, 101.02, 146.72, 147.31, 150.61, 157.30, 167.61. HRMS (ESI) C₁₃H₁₉N₆O₅ (M + H⁺) requires 339.1411, found 339.1408.

4-Amino-6-(benzylamino)-7-((2R,3R,4S,5R)-3,4-dihydroxy-5-(hydroxymethyl)tetrahydrofuran-2-yl)-7H-pyrrolo[2,3-d]pyrimidine-5-carbonitrile 14. (2R,3R,4R,5R)-2-(4-Amino-6-bromo-5-cyano-7H-pyrrolo[2,3-d]pyrimidin-7-yl)-5-((benzoyloxy)methyl)-tetrahydrofuran-3,4-diyl dibenzoate **11** (31 mg, 0.045 mmol) was dissolved in EtOH (2.0 mL), and benzylamine (29 mg, 0.27 mmol) was added to the solution. The reaction was heated in a microwave reactor at 160 °C for 1 h. After this time, the mixture was cooled to room temperature and the solvent removed under reduced pressure. The resulting residue was dissolved in methanol (0.5 mL), and 0.5 M sodium methoxide (1.0 mL) was added. The reaction was stirred at room temperature for 1 h, then the solvent was removed under reduced pressure. The resulting residue was purified by silica gel chromatography with the Biotage SP1 purification system (column, 10+S; flow rate, 15 mL/min; gradient starting with 100% DCM from 0 to 1 CV then from 100% DCM to 2% NH₄OH/18% MeOH/80% DCM from 1 CV to 21 CV) to give the desired compound as a white solid (0.007 g, 39% yield); δ H (500 MHz, MeOD) 3.80–3.86 (m, 2H), 4.18 (q, J = 1.8 Hz, 1H), 4.28 (dd, J = 5.6, 1.7 Hz, 1H), 4.73 (dd, J = 7.8, 5.7 Hz, 1H), 4.78 (d, J = 10.3 Hz, 2H), 6.37 (d, J = 7.9 Hz, 1H), 7.25–7.27 (m, 1H), 7.33–7.36 (m, 2H), 7.41–7.43 (m, 2H), 8.01 (s, 1H); δ C (126 MHz, MeOD) 46.28, 61.40, 71.14, 71.29, 86.27, 86.81, 87.38, 101.06, 118.30, 126.72, 126.98, 128.25, 138.41, 148.25, 149.94, 150.10, 154.22. HRMS (ESI) C₁₉H₂₁N₆O₄ (M + H⁺) requires 397.1619, found 397.1614.

(2R,3R,4S,5R)-2-(6-Amino-8-(benzylamino)-9H-purin-9-yl)-5-(hydroxymethyl)tetrahydrofuran-3,4-diol 15. To a solution of 8-bromoadenosine (0.061 g, 0.18 mmol) in *n*-butanol (1.76 mL) was added ⁱPr₂NEt (0.092 mL, 0.53 mmol) and benzylamine (0.038 mL, 0.35 mmol), and the mixture was heated to 120 °C for ~16 h. After this time, the mixture was cooled to room temperature and the resulting residue was purified by silica gel chromatography eluting with EtOAc:MeOH (95:5) to give the desired product as a white solid (0.017 g, 26%); δ H (500 MHz, MeOD) 8.00 (s, 1H), 7.45–7.38 (m, 2H), 7.37–7.32 (m, 2H), 7.28–7.23 (m, 1H), 6.11 (d, J = 7.7 Hz, 1H), 4.81 (dd, J = 7.6, 5.4 Hz, 1H), 4.69 (d, J = 15.8 Hz, 1H), 4.64 (d, J = 15.8 Hz, 1H), 4.30 (dd, J = 5.6, 1.6 Hz, 1H), 4.18 (q, J = 1.9 Hz, 1H), 3.85 (dd, J = 12.0, 2.3 Hz, 1H), 3.79 (dd, J = 11.9, 1.7 Hz, 1H); δ C (126 MHz, MeOD) 152.12, 151.99, 149.65, 148.63, 138.75, 128.11, 126.68, 126.52, 116.56, 87.29, 86.41, 71.64, 71.52, 61.75, 45.42. HRMS (ESI) C₁₇H₂₁N₆O₄ (M + H⁺) requires 373.1623.

(2R,3R,4S,5R)-2-(6-Amino-8-((quinolin-6-ylmethyl)amino)-9H-purin-9-yl)-5-(hydroxymethyl)tetrahydrofuran-3,4-diol 17. To a solution of 8-bromoadenosine (0.099 g, 0.29 mmol) in *n*-butanol (2.9 mL) was added quinolin-6-ylmethanamine (0.045 g, 0.29 mmol) and ⁱPr₂NEt (0.15 mL, 0.85 mmol), and the mixture was heated to 120 °C under N₂ for 24 h. After this time, the mixture was cooled to room temperature and the solvent removed under reduced pressure. The resulting residue was purified by chromatography eluting with EtOAc:2 M MeOH/NH₃ (80:20) to give the desired product as a white solid (0.008 g, 7%); δ H (500 MHz, MeOD) 8.83 (dd, J = 4.4, 1.7 Hz, 1H), 8.37 (dt, J = 8.4, 1.2 Hz, 1H), 8.04 (d, J = 8.7 Hz, 1H),

8.02 (s, 1H), 7.95 (d, J = 1.8 Hz, 1H), 7.86 (dd, J = 8.8, 2.0 Hz, 1H), 7.54 (dd, J = 8.3, 4.3 Hz, 1H), 6.16 (d, J = 7.6 Hz, 1H), 4.92–4.83 (obs m, 3H), 4.32 (dd, J = 5.4, 1.7 Hz, 1H), 4.21 (q, J = 1.9 Hz, 1H), 3.87 (dd, J = 12.0, 2.3 Hz, 1H), 3.80 (dd, J = 11.9, 1.7 Hz, 1H); δ C (126 MHz, MeOD) 151.98, 151.94, 149.72, 149.52, 148.44, 146.69, 137.89, 136.94, 129.30, 128.46, 127.90, 125.07, 121.35, 116.59, 87.38, 86.47, 71.70, 71.53, 61.75, 45.29. HRMS (ESI) C₂₀H₂₂N₇O₄ (M + H⁺) requires 424.1728, found 424.1725.

(2R,3R,4S,5R)-2-(6-Amino-8-((4-chlorobenzyl)amino)-9H-purin-9-yl)-5-(hydroxymethyl)tetrahydrofuran-3,4-diol 18. To a solution of 8-bromoadenosine (0.078 g, 0.23 mmol) in *n*-butanol (2.3 mL) was added ⁱPr₂NEt (0.12 mL, 0.68 mmol) and (4-chlorophenyl)methanamine (0.055 mL, 0.45 mmol), and the mixture was heated to 120 °C for ~12 h. After this time, the mixture was cooled to room temperature and the resulting residue was purified by silica gel chromatography eluting with EtOAc:MeOH (95:5) to give the desired product as a white solid (0.033 g, 36%); δ H (500 MHz, MeOD) 8.00 (s, 1H), 7.40 (d, J = 8.3 Hz, 2H), 7.35 (d, J = 8.6 Hz, 2H), 6.10 (d, J = 7.5 Hz, 1H), 4.79 (dd, J = 7.6, 5.4 Hz, 1H), 4.66 (d, J = 15.9 Hz, 1H), 4.62 (d, J = 16.0 Hz, 1H), 4.30 (dd, J = 5.4, 1.7 Hz, 1H), 4.18 (q, J = 1.9 Hz, 1H), 3.85 (dd, J = 11.9, 2.3 Hz, 1H), 3.79 (dd, J = 12.0, 1.7 Hz, 1H); δ C (126 MHz, MeOD) 152.19, 151.83, 149.68, 148.72, 137.67, 132.42, 128.22, 128.16, 116.54, 87.30, 86.40, 71.65, 71.50, 61.73, 44.80. HRMS (ESI) C₁₇H₂₀ClN₆O₄ (M+H⁺) requires 407.1229, found 407.1237.

(2R,3R,4S,5R)-2-(6-Amino-8-((4-fluorobenzyl)amino)-9H-purin-9-yl)-5-(hydroxymethyl)tetrahydrofuran-3,4-diol 19. To a solution of 8-bromoadenosine (0.048 g, 0.14 mmol) in *n*-butanol (1.4 mL) was added (4-fluorophenyl)methanamine (0.032 mL, 0.28 mmol) and ⁱPr₂NEt (0.073 mL, 0.42 mmol), and the mixture was heated to 120 °C for ~12 h. After this time, the mixture was cooled to room temperature and the solvent removed under reduced pressure. The resulting residue was purified by silica gel chromatography eluting with EtOAc:MeOH (9:1) to give the desired product as a white solid (0.043 g, 79%); δ H (500 MHz, MeOD) 7.99 (s, 1H), 7.50 (dd, J = 8.3, 5.3 Hz, 1H), 7.44–7.38 (m, 2H), 7.23–7.16 (m, 1H), 7.09–7.04 (m, 2H), 6.09 (d, J = 7.6 Hz, 1H), 4.78 (dd, J = 7.6, 5.4 Hz, 1H), 4.65 (d, J = 15.7 Hz, 1H), 4.60 (d, J = 15.7 Hz, 1H), 4.29 (dd, J = 5.4, 1.6 Hz, 1H), 4.17 (q, J = 1.9 Hz, 1H), 3.83 (dd, J = 12.0, 2.2 Hz, 1H), 3.78 (dd, J = 11.9, 1.7 Hz, 1H); δ C (126 MHz, MeOD) 164.14, 163.00, 161.06, 152.14, 151.85, 149.66, 148.65, 134.75, 134.72, 130.99, 130.92, 128.53, 128.46, 116.55, 115.67, 115.50, 114.79, 114.62, 87.26, 86.41, 71.60, 71.50, 61.72, 44.79.⁴³ HRMS (ESI) C₁₇H₂₀FN₆O₄ (M + H⁺) requires 391.1525, found 391.1517.

(2R,3R,4S,5R)-2-(6-Amino-8-((4-methylbenzyl)amino)-9H-purin-9-yl)-5-(hydroxymethyl)tetrahydrofuran-3,4-diol 20. To a solution of 8-bromoadenosine (0.062 g, 0.18 mmol) in *n*-butanol (1.79 mL) was added *p*-tolylmethanamine (0.045 mL, 0.36 mmol) and ⁱPr₂NEt (0.093 mL, 0.54 mmol), and the mixture was heated to 120 °C for ~48 h. After this time, the mixture was cooled to room temperature and the solvent removed under reduced pressure. The resulting residue was purified by silica gel chromatography eluting with EtOAc:MeOH (9:1) to give the desired product as a white solid (0.042 g, 61%); δ H (500 MHz, MeOD) 7.99 (s, 1H), 7.28 (d, J = 7.8 Hz, 2H), 7.16 (d, J = 7.7 Hz, 2H), 6.09 (d, J = 7.6 Hz, 1H), 4.80 (dd, J = 7.6, 5.4 Hz, 1H), 4.64 (d, J = 15.6 Hz, 1H), 4.58 (d, J = 15.6 Hz, 1H), 4.29 (dd, J = 5.4, 1.7 Hz, 1H), 4.18 (d, J = 1.9 Hz, 1H), 3.84 (dd, J = 12.0, 2.3 Hz, 1H), 3.78 (dd, J = 11.9, 1.7 Hz, 1H), 2.32 (s, 3H); δ C (126 MHz, MeOD) 152.08, 152.01, 149.64, 148.59, 136.39, 135.64, 128.70, 126.57, 116.57, 87.27, 86.40, 71.61, 71.50, 61.74, 45.26, 19.70. HRMS (ESI) C₁₈H₂₃N₆O₄ (M + H⁺) requires 387.1775, found 387.1779.

(2R,3R,4S,5R)-2-(6-Amino-8-((3,4-dichlorobenzyl)amino)-9H-purin-9-yl)-5-(hydroxymethyl)tetrahydrofuran-3,4-diol 21. To a microwave vial was added 8-bromoadenosine (0.30 g, 0.27 mmol) and 3,4-dichlorobenzylamine (0.29 mL, 2.2 mmol) in ethanol (1.7 mL). The reaction mixture was irradiated at 140 °C for 90 min. The reaction mixture was concentrated, and the crude residue was purified by silica gel column chromatography eluting with EtOH:DCM (3:7) to give the desired product as a white solid (0.28 g, 73%); δ H (500

MHz, DMSO- d_6) 7.90 (s, 1H), 7.70–7.53 (m, 3H), 7.37 (dd, $J = 8.3$, 2.0 Hz, 1H), 6.55 (s, 2H), 5.99–5.85 (m, 2H), 5.32 (d, $J = 6.6$ Hz, 1H), 5.18 (d, $J = 4.0$ Hz, 1H), 4.72 (td, $J = 7.0$, 5.3 Hz, 1H), 4.56 (d, $J = 6.0$ Hz, 2H), 4.12 (ddd, $J = 5.5$, 3.9, 1.9 Hz, 1H), 3.99 (q, $J = 2.3$ Hz, 1H), 3.62 (dt, $J = 7.0$, 3.2 Hz, 2H) 3.45–3.35 (obs. m, 1H); δC (126 MHz, DMSO- d_6) 153.01, 151.48, 150.25, 149.17, 141.70, 131.27, 130.86, 129.66, 129.58, 128.05, 117.38, 87.00, 86.30, 71.53, 71.38, 62.23, 44.76. HRMS (ESI) $C_{17}H_{19}Cl_2N_6O_4$ ($M + H^+$) requires 442.0867, found 442.0859.

(2*R*,3*R*,4*S*,5*R*)-2-(6-Amino-8-((4-methoxybenzyl)amino)-9H-purin-9-yl)-5-(hydroxymethyl)tetrahydrofuran-3,4-diol **22**. To a solution of 8-bromoadenosine (0.073 g, 0.21 mmol) in *n*-butanol (4.2 mL) was added (4-methoxyphenyl)methanamine (0.083 mL, 0.63 mmol) and 3Pr_2NEt (0.22 mL, 1.3 mmol), and the mixture was heated to 120 °C for ~12 h. After this time, the mixture was cooled to room temperature and the solvent removed under reduced pressure. The resulting residue was purified by silica gel chromatography eluting with EtOAc:MeOH (95:5) to give the desired product as a white solid (0.049 g, 58%); δH (500 MHz, MeOD) 7.98 (s, 1H), 7.32 (d, $J = 8.8$ Hz, 2H), 6.89 (d, $J = 8.8$ Hz, 2H), 6.07 (d, $J = 7.6$ Hz, 1H), 4.78 (dd, $J = 7.6$, 5.4 Hz, 1H), 4.60 (d, $J = 15.3$ Hz, 2H), 4.55 (d, $J = 15.3$ Hz, 1H), 4.28 (dd, $J = 5.6$, 1.7 Hz, 1H), 4.16 (q, $J = 1.9$ Hz, 1H), 3.83 (dd, $J = 12.0$, 2.3 Hz, 1H), 3.78 (s, 3H), 3.77 (obs. dd, $J = 11.9$, 1.7 Hz, 1H); δC (126 MHz, MeOD) 158.96, 152.09, 151.98, 149.63, 148.59, 130.63, 127.94, 116.59, 113.49, 87.27, 86.38, 71.61, 71.48, 61.73, 54.26, 45.05. HRMS (ESI) $C_{18}H_{22}N_6NaO_5$ ($M + Na^+$) requires 425.1544, found 425.1540.

Experimental Procedures (Surface Plasmon Resonance Spectroscopy). All surface plasmon resonance (SPR) experiments were carried out on a Biacore T100 enhanced to T200 sensitivity (GE Life Sciences, Amersham Place, UK). Amine coupling chemistry was used to immobilize the truncated HSC70-NBD domain (residues 1–381) on a research grade CMS sensor chip. The running buffer used in the immobilization step consisted of 1× phosphate buffered saline (10 mM NaH_2PO_4/NaH_2PO_4 pH 7.4, 2.7 mM KCl, 137 mM NaCl), and the chip surface was activated for 10 min using a 1:1 mixture of 100 mM *N*-hydroxysuccinimide and 400 mM 1-ethyl-3-(3-(dimethylamino)propyl)-carbodiimide. HSC70-NBD was injected at a concentration of 70 $\mu g/mL$ in a 10 mM acetate buffer pH 5.0 with 750 μM ADP as protection for the active site lysines. The reaction was monitored in real time and stopped when a target immobilization level of ~5000RU was obtained. Finally, the surface was blocked via an injection of 1 M ethanolamine at pH 8.5 for 7 min. The flow rate was maintained at 10 $\mu L/min$ for all the above procedures. Flow cell one was left unmodified and used as the reference surface.

Following protein immobilization, the running buffer was changed to 1× phosphate buffered saline containing 0.05% (v/v) Tween20 and 5% (v/v) DMSO in order to reduce the nonspecific binding and increase solubility of the compounds.

All liquid handling was carried out using an ECHO 550 acoustic liquid dispenser (Labcyte, Dublin, Ireland), and compounds were added to 384-well polypropylene V-bottomed plates (Greiner, Stonehouse, UK), which were used as sample plates for the SPR experiments. For each compound, an eight-point dose response experiment was carried out using a concentration range of 50–2000 μM , 5–200 μM or 0.0625–2.5 μM , depending on the potency of the compound. The buffer mix was made compatible with the Biacore running buffer. The experiments were performed at a flow rate of 30 $\mu L/min$, a sample injection time of 60 s, and a dissociation time of 120 s. The CMS surface was not regenerated between sample injections.

K_D values were calculated from the background normalized binding curve generated from the sensorgrams under equilibrium conditions, using the 1:1 binding model in the Biacore software version 2 (GE Life Sciences, Amersham Place, UK). All results are reported as the geometric mean \pm standard error of the mean (SEM) of at least three independent measurements unless otherwise stated. The ratio of experimental to theoretical RU_{max} varied from 0.84 to 1.40. Examples of sensorgrams and binding curves can be found in the Supporting Information.

Experimental Procedure (HSP72-NBD Protein Preparation).

The human HSPA1A (HSP72) gene was amplified from the IMAGE clone 3345864 (accession no. BC002453) by PCR using the respective forward and reverse primers 5'-GATCGACCATATGGCCAAAGCCGCGGCGA-3' and 5'-ACAGAATTCCTAATCTACTCTCTCAATGG-3'. The HSPA1A gene was cloned into a pTWOE vector, which is a modified version of pET-17b (Merck Chemicals Ltd., Nottingham, UK) encoding a N-terminal 6xHis-tag followed by a human rhinovirus 3C protease cleavage site. BL21-AI cells (Invitrogen, Paisley, UK) transformed with the vector containing the HSPA1A gene were grown in Luria–Bertani medium to an optical density at 600 nm of 0.6 and induced with 0.5 mM isopropyl- β -D-1-thiogalactopyranoside and 0.2% (w/v) arabinose at for 16 h at 20 °C. Cells were harvested by centrifugation at 6000 rpm for 40 min at 4 °C using an Avanti centrifuge J-26XP (Beckman Coulter, High Wycombe, UK) with a JLA 8.100 rotor. Cell pellets were resuspended in 3 volumes of lysis buffer consisting of 25 mM Tris, 50 mM NaCl, 5% (v/v) glycerol, 1× cComplete EDTA-free protease inhibitors (Roche, Basel, Switzerland), 25 U/mL benzonase nuclease (Merck Chemicals Ltd.) at pH 7.5. Cell lysis was performed by sonication using a Vibra-Cell VCX500 (Sonics & Materials Inc., Newtown, CT, USA) with a 13 mm solid probe for 24 cycles of 5 s on, 55 s off with amplitude set at 50%. The lysate was clarified by centrifugation at 20000 rpm for 30 min at 4 °C using an Avanti centrifuge J-26XP (Beckman Coulter) with a JA 25.50 rotor.

The supernatant was passed through a 1.2 μm syringe filter (Sartorius Stedim, Germany) and loaded onto a 5 mL Histrap FF column (GE Healthcare, Chalfont St. Giles, UK) equilibrated in buffer A, comprising 25 mM Tris, 50 mM NaCl, pH 7.5, and eluted with a gradient of 0–100% buffer B (buffer A + 250 mM imidazole) over 10 column volumes (CV). Fractions containing HSP72 were pooled, concentrated, and loaded onto a Superdex 200 (16/60) size exclusion column (GE Healthcare) equilibrated in 25 mM Tris, 400 mM NaCl, 2 mM EDTA 5% (v/v) glycerol, pH 7.5, for further purification. Fractions containing HSP72 were pooled and further purified to remove contaminating nucleotides using a 6 mL Resource Q column (GE Healthcare) equilibrated in 20 mM Tris, 2 mM EDTA, 5% (v/v) glycerol, pH 7.5. Following a 10 CV wash with the same buffer, HSP72 was eluted using a gradient from 0 to 500 mM NaCl over 6 CV and loaded onto a Superdex 200 16/60 column (GE Healthcare) equilibrated in a buffer containing 25 mM Tris, 400 mM NaCl, 15 mM EDTA, 5% (v/v) glycerol, pH 7.5. The removal of contaminating nucleotides was followed by measuring the ratio of absorbance at 260 and 280 nm (A_{260}/A_{280}) using a NanoDrop ND-1000 UV spectrophotometer (ThermoFisher, Wilmington, DE, USA). Samples with A_{260}/A_{280} below 0.6 were regarded as nucleotide free.

Experimental Procedure (X-ray Crystallography). Purified HSP72-NBD protein was thawed; buffer exchanged into fresh 100 mM HEPES pH 7.5 and incubated with 5 mM of the inhibitor for 30 min on ice prior to crystallization. HSP72-NBD/inhibitor co-crystals were grown at 18 °C in sitting drops by mixing equal volumes of protein solution (5–12 mg/mL) and precipitant solution containing 17–28% (v/v) PEG3350, 0.1 M HEPES pH 7.5, 2 mM $MgCl_2$, and 2 mM NaH_2PO_4 . Co-crystals of approximate dimensions 100 \times 100 \times 300 μm^3 typically formed overnight. Crystals were in liquid nitrogen, using 22.5% (v/v) ethylene glycol for the co-crystals with sangivamycin **10** and 25% (v/v) glycerol for compound **17**.

X-ray diffraction data were collected at 100 K at Diamond Light Source (Oxfordshire, UK; beamlines I04–1 and I24). Data were integrated with XDS. All data were imported to MTZ format with POINTLESS, then scaled and merged with AIMLESS and the CCP4 suite. The structures were solved by molecular replacement with PHASER, with the public domain HSP72-NBD structure 1S3X as the search model after removal of all nonprotein atoms. Structures were refined in iterative cycles of model building with COOT and refinement with BUSTER. TLS groups were selected with PHENIX phenix.find_tls_groups. Ligand restraints were generated with GRADE and MOGUL. The final structure quality was checked with MOLPROBITY. The data collection and refinement statistics are presented in Supporting Information Table S15, and for $F_o - F_c$

electron density figures for all structural data, see Supporting Information Figure S14. $F_o - F_c$ electron density figures were generated with CCP4MG.

■ ASSOCIATED CONTENT

📄 Supporting Information

The Supporting Information is available free of charge on the ACS Publications website at DOI: 10.1021/acs.jmedchem.5b02001.

Details of commercially available adenosine analogues, table of HSP70 affinities, NMR spectra of final compounds, representative SPR sensorgrams and binding curves, $F_o - F_c$ electron density for ligand-bound HSP72 crystal structures, data collection and refinement statistics for HSP72 co-crystal structures with ligands, overlays of the co-crystal structures highlighting key residues (PDF)

Molecular formula strings (CSV)

Accession Codes

Atomic coordinates and structure factors for the crystal structures of HSP72-NBD with compounds can be accessed using PDB codes: 10 5AQQ, 17 5AR0. Authors will release the atomic coordinates and experimental data upon article publication.

■ AUTHOR INFORMATION

Corresponding Author

*Phone: +44 (0) 20 8722 4334. E-mail: keith.jones@icr.ac.uk.

Author Contributions

The manuscript was written through contributions of all authors. All authors have given approval to the final version of the manuscript.

Notes

The authors declare no competing financial interest.

■ ACKNOWLEDGMENTS

This work was supported by Cancer Research UK grant nos. C309/A8274 and C309/A11566. We acknowledge NHS funding to the NIHR Biomedical Research Centre at The Institute of Cancer Research and the Royal Marsden Hospital. We thank Dr. Nora Cronin and the staff of DIAMOND Light Source for their support during data collection.

■ ABBREVIATIONS USED

HSP90, heat-shock protein 90; HSP70, heat-shock protein 70; HSP72, heat-shock protein 72; HSC70, heat-shock cognate 70; HSP40, heat-shock protein 40, chaperone DnaJ; BAG1, BAG family molecular chaperone regulator 1; ATP, adenosine triphosphate; ADP, adenosine diphosphate; P_i , inorganic phosphate; K_D , equilibrium dissociation constant; pK_D , negative \log_{10} of the equilibrium dissociation constant; SEM, standard error of the mean; SAR, structure–activity relationship; μM , micromolar; n, number of statistical repeats; NBD, nucleotide-binding domain; SPR, surface plasmon resonance

■ REFERENCES

(1) Hartl, F. U.; Bracher, A.; Hayer-Hartl, M. Molecular chaperones in protein folding and proteostasis. *Nature* **2011**, *475*, 324–332.
(2) Powers, M. V.; Workman, P. Inhibitors of the heat-shock response: biology and pharmacology. *FEBS Lett.* **2007**, *581*, 3758–3769.

(3) (a) Garcia-Carbonero, R.; Carnero, A.; Paz-Ares, L. Inhibition of HSP90 molecular chaperones: moving into the clinic. *Lancet Oncol.* **2013**, *14*, e358–e369. (b) Butler, L. M.; Ferraldeschi, R.; Armstrong, H. K.; Centenera, M. M.; Workman, P. Maximizing the Therapeutic Potential of HSP90 Inhibitors. *Mol. Cancer Res.* **2015**, *13*, 1445–1451.

(4) Powers, M. V.; Jones, K.; Barillari, C.; Westwood, I.; van Montfort, R. L. M.; Workman, P. Targeting HSP70: the second potentially druggable heat shock protein and molecular chaperone? *Cell Cycle* **2010**, *9*, 1542–1550.

(5) Powers, M. V.; Clarke, P. A.; Workman, P. Dual targeting of HSC70 and HSP72 inhibits HSP90 function and induces tumor-specific apoptosis. *Cancer Cell* **2008**, *14*, 250–262.

(6) (a) Mayer, M. P.; Bukau, B. HSP70 Chaperones: cellular functions and molecular mechanism. *Cell. Mol. Life Sci.* **2005**, *62*, 670–684. (b) Laufen, T.; Mayer, M. P.; Beisel, C.; Klostermeier, D.; Mogk, A.; Reinstein, J.; Bukau, B. Mechanism of regulation of HSP70 chaperones by DnaJ cochaperones. *Proc. Natl. Acad. Sci. U. S. A.* **1999**, *96*, 5452–5457.

(7) (a) Williamson, D. S.; Borgognoni, J.; Clay, A.; Daniels, Z.; Dokurno, P.; Drysdale, M. J.; Foloppe, N.; Francis, G. L.; Graham, C. J.; Howes, R.; Macias, A. T.; Murray, J. B.; Parsons, R.; Shaw, T.; Surgenor, A. E.; Terry, L.; Wang, Y.; Wood, M.; Massey, A. J. Novel adenosine-derived inhibitors of 70 KDa heat shock protein, discovered through structure-based design. *J. Med. Chem.* **2009**, *52*, 1510–1513. (b) Macias, A. T.; Williamson, D. S.; Allen, N.; Borgognoni, J.; Clay, A.; Daniels, Z.; Dokurno, P.; Drysdale, M. J.; Francis, G. L.; Graham, C. J.; Howes, R.; Matassova, N.; Murray, J. B.; Parsons, R.; Shaw, T.; Surgenor, A. E.; Terry, L.; Wang, Y.; Wood, M.; Massey, A. J. Adenosine-derived inhibitors of 78 KDa glucose regulated protein (GRP78) ATPase: insights into isoform selectivity. *J. Med. Chem.* **2011**, *54*, 4034–4041.

(8) Several non-ATP competitive inhibitors have been described in the literature see: (a) Fewell, S. W.; Day, B. W.; Brodsky, J. L. Identification of an inhibitor of HSC70-mediated protein translocation and ATP hydrolysis. *J. Biol. Chem.* **2001**, *276*, 910–914. (b) Fewell, S. W.; Smith, C. M.; Lyon, M. A.; Dumitrescu, T. P.; Wipf, P.; Day, W. W.; Brodsky, J. L. Small molecule modulators of endogenous and co-chaperone stimulated HSP70 ATPase activity. *J. Biol. Chem.* **2004**, *279*, 51131–51140. (c) Rousaki, A.; Miyata, Y.; Jinwal, U. K.; Dickey, C. A.; Gestwicki, J. E.; Zuiderweg, E. R. Allosteric drugs: the interaction of antitumor compound MKT-077 with human HSP70 chaperones. *J. Mol. Biol.* **2011**, *411*, 614–632. (d) Williams, D. R.; Ko, S. K.; Park, S.; Lee, M. R.; Shin, I. An apoptosis-inducing small molecule that binds to heat shock protein 70. *Angew. Chem., Int. Ed.* **2008**, *47*, 7466–7469. (e) Jinwal, U. K.; Miyata, Y.; Koren, J.; Jones, J. R.; Trotter, J. H.; Chang, L.; O'Leary, J.; Morgan, D.; Lee, D. C.; Shults, C. L.; Rousaki, A.; Weeber, E. J.; Zuiderweg, E. R. P.; Gestwicki, J. E.; Dickey, C. A. Chemical manipulation of HSP70 ATPase activity regulates tau stability. *J. Neurosci.* **2009**, *29*, 12079–12088. (f) Miyata, Y.; Rauch, J. N.; Jinwal, U. K.; Thompson, A. D.; Srinivasan, S.; Dickey, C. A.; Gestwicki, J. E. Cysteine reactivity distinguishes redox sensing by the heat inducible and constitutive forms of heat shock protein 70 (HSP70). *Chem. Biol.* **2012**, *19*, 1391–1399. (g) Howe, M. K.; Bodoor, K.; Carlson, D. A.; Hughes, P. F.; Alwarawrah, Y.; Loiselle, D. R.; Jaeger, A. M.; Darr, D. B.; Jordan, J. L.; Hunter, L. M.; Molzberger, E. T.; Gobillot, T. A.; Thiele, D. J.; Brodsky, J. L.; Spector, N. L.; Haystead, T. A. J. Identification of an allosteric small-molecule inhibitor selective for the inducible form of heat shock protein 70. *Chem. Biol.* **2014**, *21*, 1648–1659. (h) Dal Piaz, F.; Cotugno, R.; Lepore, L.; Vassallo, A.; Malafrente, N.; Lauro, G.; Bifulco, G.; Belisario, M. A.; De Tommasi, N. Chemical proteomics reveals HSP70 1A as a target for the anticancer diterpene oridonin in jurkat cells. *J. Proteomics* **2013**, *82*, 14–26. (i) Rodina, A.; Patel, P. D.; Kang, Y.; Patel, Y.; Baaklini, I.; Wong, M. J.; Taldone, T.; Yan, P.; Yang, C.; Maharaj, R.; Gozman, A.; Patel, M. R.; Patel, H. J.; Chirico, W.; Erdjument-Bromage, H.; Talele, T. T.; Young, J. C.; Chiosis, G. Identification of an allosteric pocket on human HSP70 reveals a mode of inhibition of this therapeutically important protein. *Chem. Biol.* **2013**, *20*, 1469–1480. (j) Hassan, A. Q.; Kirby, C. A.; Zhou, W.;

Schuhmann, T.; Kityk, R.; Kipp, D. R.; Baird, J.; Chen, J.; Chen, Y.; Chung, F.; Hoepfner, D.; Movva, N. R.; Pagliarini, R.; Petersen, F.; Quinn, C.; Quinn, D.; Riedl, R.; Schmitt, E. K.; Schitter, A.; Stams, T.; Studer, C.; Fortin, P. D.; Mayer, M. P.; Sadlish, H. The novolactone natural product disrupts the allosteric regulation of HSP70. *Chem. Biol.* **2015**, *22*, 87–97.

(9) Recently, a set of novel piperidine derivatives as inhibitors of HSP70 but is unclear whether the cellular effects can be attributed HSP70 inhibition. Zeng, Y.; Cao, R.; Zhang, T.; Li, S.; Zhong, W. Design and synthesis of piperidine derivatives as novel human heat shock protein 70 inhibitors for the treatment of drug-resistant tumors. *Eur. J. Med. Chem.* **2015**, *97*, 19–31.

(10) The validity of two HSP70 inhibitors have recently been investigated: (a) Schlecht, R.; Scholz, S. R.; Dahmen, H.; Wegener, A.; Sirrenberg, C.; Musil, D.; Bomke, J.; Eggenweiler, H. M.; Mayer, M. P.; Bukau, B. Functional analysis of HSP70 inhibitors. *PLoS One* **2013**, *8*, e78443. (b) Evans, L. E.; Cheeseman, M. D.; Yahya, N.; Jones, K. Investigating apozazole as a chemical probe for HSP70 inhibition. *PLoS One* **2015**, *10*, e0140006.

(11) (a) Bork, P.; Sander, C.; Valencia, A. An ATPase domain common to prokaryotic cell cycle proteins, sugar kinases, actin, and HSP70 heat shock proteins. *Proc. Natl. Acad. Sci. U. S. A.* **1992**, *89*, 7290–7294. (b) Flaherty, K. M.; McKay, D. B.; Kabsch, W.; Holmes, K. Similarity of the three-dimensional structures of actin and the ATPase fragment of a 70-KDa heat shock cognate protein. *Proc. Natl. Acad. Sci. U. S. A.* **1991**, *88*, 5041–5045. (c) Chene, P. ATPases as drug targets: learning from their structure. *Nat. Rev. Drug Discovery* **2002**, *1*, 665–673.

(12) Massey, A. J. ATPases as drug targets: insights from heat shock proteins 70 and 90. *J. Med. Chem.* **2010**, *53*, 7280–7286.

(13) SiteMap, version 2.2; Schrodinger LLC: 120 West 45th Street, New York, NY 10036, 2008.

(14) HSP70 is quoted as returning a Dscore = 0.95, classifying the target as “difficult”, see reference 12 and Halgren, T. A. Identifying and characterizing binding sites and assessing drugability. *J. Chem. Inf. Model.* **2009**, *49*, 377–389.

(15) This analysis was carried out by Vernalis using their fragment screening deck; see reference 12 and Hajduk, P. J.; Huth, J. R.; Fesik, S. W. Drugability indices for protein targets derived from NMR-based screening data. *J. Med. Chem.* **2005**, *48*, 2518–2525.

(16) (a) Arakawa, A.; Handa, N.; Ohsawa, N.; Shida, M.; Kigawa, T.; Hayashi, F.; Shirouzu, M.; Yokoyama, S. The C-terminal BAG domain of BAG5 induces conformational changes of the HSP70 nucleotide-binding domain for ADP-ATP exchange. *Structure* **2010**, *18*, 309–319. (b) Vogel, M.; Bukau, B.; Mayer, M. P. Allosteric regulation of HSP70 chaperones by a proline switch. *Mol. Cell* **2006**, *21*, 359–367. (c) Rist, W.; Graf, C.; Bukau, B.; Mayer, M. P. Amide hydrogen exchange reveals conformational changes in HSP70 chaperones important for allosteric regulation. *J. Biol. Chem.* **2006**, *281*, 16493–16501. (d) Mayer, M. P.; Bukau, B. HSP70 chaperones: cellular functions and molecular mechanism. *Cell. Mol. Life Sci.* **2005**, *62*, 670–684.

(17) The off-rate of ADP/P_i from HSP72 has been calculated using MABA-ADP and is ~0.05 s⁻¹, the steady state ATPase rate in the absence of co-chaperones has been calculated as ~4.5 × 10⁻⁴ s⁻¹, see: Gassler, C. S.; Wiederkehr, T.; Brehmer, D.; Bukau, B.; Mayer, M. P. BAG-1M accelerates nucleotide release for human HSC70 and HSP70 and can act concentration-dependent as positive and negative cofactor. *J. Biol. Chem.* **2001**, *276* (35), 32538–32544.

(18) For more details see the Supporting Information.

(19) All SPR data was measured with the Biacore T200 instrument using the analysis software (version 2) provided. HSC70-NBD was loaded on to the series S CMS sensor chip as per the manufacturer's instructions and in the presence of 750 μM ADP to protect active site lysines. pK_D = -log₁₀[K_D(μM) × 10⁻⁶]. All results are the geometric mean ± SEM of three independent experiments measured at similar protein binding levels (~5000 RU). The K_D values were determined from analysis of the background normalized binding curve generated from the sensorgrams under equilibrium conditions using a 1:1 binding model. For all experiments, the ratio of experimental RU_{max} to

theoretical RU_{max} was approximately 1. Representative examples of sensorgrams and binding curves can be found in the Supporting Information.

(20) Standard adenosine and adenine numbering system is used throughout this publication.

(21) This data can be observed in the Supporting Information.

(22) All fold differences that are quoted are statistically significant at the 95% level using Student's *t*-test, see: Cumming, G.; Fidler, F.; Vaux, D. L. Error bars in experimental biology. *J. Cell Biol.* **2007**, *177*, 7–11.

(23) Stumpfe, D.; Hu, Y.; Dimova, D.; Bajorath, J. Recent progress in understanding activity cliffs and their utility in medicinal chemistry. *J. Med. Chem.* **2014**, *57*, 18–28.

(24) Jiang, L.; Mao, X.-A. Conformations of adenosine-5'-triphosphate in the presence of Mg²⁺ at different pH. *Polyhedron* **2002**, *21*, 435–438.

(25) Adenosine numbering system used throughout for comparison.

(26) See Supporting Information for purchasing details of commercially available natural products used in this study.

(27) Gunic, E.; Girardet, J.; Pietrzakowski, Z.; Esler, C.; Wang, G. Synthesis and cytotoxicity of 4'-C- and 5'-C-substituted toyocamycins. *Bioorg. Med. Chem.* **2001**, *9*, 163–170.

(28) 8-N-Methylaminosangivamycin 13 could only be isolated in 80% purity and was tested at this level of purity in subsequent assays.

(29) Because of the low yield and purity in the synthesis of 13, there was only sufficient material to do a single SPR analysis to measure the compound's affinity to HSP70.

(30) Kuhn, B.; Mohr, P.; Stahl, M. Intramolecular hydrogen bonding in medicinal chemistry. *J. Med. Chem.* **2010**, *53*, 2601–2611.

(31) Minamoto, K.; Fujiki, Y.; Shiomi, N.; Uda, Y.; Sasaki, T. Systematic general synthesis of purine 8,5'-imino and substituted imino cyclonucleosides. *J. Chem. Soc., Perkin Trans. 1* **1985**, *11*, 2337–2346.

(32) Ha, J.; McKay, D. B. Kinetics of nucleotide-induced changes in the tryptophan fluorescence of the molecular chaperone HSC70 and its subfragments suggest the ATP-induced conformational change follows initial ATP binding. *Biochemistry* **1995**, *34*, 11635–11644.

(33) For a discussion on the effect of binding mechanism and conformational change in drug discovery, see: Holdgate, G. A.; Gill, A. L. Kinetic efficiency: the missing metric for enhancing compound quality? *Drug Discovery Today* **2011**, *16*, 910–913.

(34) This result is comparable to the previously described affinity of ADP for HSP70 (K_D = 0.5 μM. See ref 7. The affinity of ADP for HSP70 is known to be highly dependent on the assay conditions, see: Arakawa, A.; Handa, N.; Shirouzu, M.; Yokoyama, S. Biochemical and structural studies on the high affinity of HSP70 for ADP. *Protein Sci.* **2011**, *20*, 1367–1379.

(35) The salt-bridge between glutamic acid-268 and lysine-56 can be observed in several other published HSP70/ADP structures, see: (a) PDB 3ATU reference 34; (b) PDB 3JXU: Wisniewska, M.; Karlberg, T.; Lehtio, L.; Johansson, I.; Kotenyova, T.; Moche, M.; Schuler, H. Crystal structures of the ATPase domains of four human HSP70 isoforms: HSPA1L/HSP70-hom, HSPA2/HSP70-2, HSPA6/HSP70B', and HSPAS/BiP/GRP78. *PLoS One* **2010**, *5*, e8625. (c) PDB 1S3X: Sriram, M.; Osipiuk, J.; Freeman, B.; Morimoto, R.; Joachimiak, A. Human HSP70 molecular chaperone binds two calcium ions within the ATPase domain. *Structure* **1997**, *5*, 403–414. (d) PDB 2E8A: Shida, M.; Arakawa, A.; Ishii, R.; Kishishita, S.; Takagi, T.; Kukimoto-Niino, M.; Sugano, S.; Tanaka, A.; Shirouzu, M.; Yokoyama, S. Direct inter-subdomain interactions switch between the closed and open forms of the HSP70 nucleotide binding domain in the nucleotide-free state. *Acta Crystallogr., Sect. D: Biol. Crystallogr.* **2010**, *66*, 223–232.

(36) Rye, C. S.; Baell, J. B. Phosphate isosteres in medicinal chemistry. *Curr. Med. Chem.* **2005**, *12*, 3127–3141.

(37) 8-N-Quinoloneaminoadenosine derived ligand 17 was previously reported to have a K_D = 0.23 μM as measured by SPR against the HSP70 isoform GRP78, see ref 7.

(38) Luo, R.; David, L.; Hung, H.; Devaney, J.; Gilson, M. K. Strength of solvent-exposed salt-bridges. *J. Phys. Chem. B* **1999**, *103*, 727–736. (b) Dong, F.; Zhou, H. Electrostatic contributions to T4 lysozyme stability: solvent-exposed charges versus semi-buried salt bridges. *Biophys. J.* **2002**, *83*, 1341–1347.

(39) Berry, B. W.; Elvekrog, M. M.; Tommos, C. Environmental modulation of protein cation- π interactions. *J. Am. Chem. Soc.* **2007**, *129* (17), 5308–5309.

(40) For a discussion on the effects of “burying” solvent exposed intramolecular hydrogen bonds and salt-bridges of proteins, see: (a) Hendsch, Z. S.; Tidor, B. Do salt bridges stabilize proteins? a continuum electrostatic analysis. *Protein Sci.* **1994**, *3*, 211–226. (b) Efimov, A.; Brazhnikov, E. V. Relationship between intramolecular hydrogen bonding and solvent accessibility of side-chain donors and acceptors in proteins. *FEBS Lett.* **2003**, *554*, 389–393.

(41) Murray, J. B.; Roughley, S. D.; Matassova, N.; Brough, P. A. Off-rate screening (ORS) by surface plasmon resonance. An efficient method to kinetically sample hit to lead chemical space from unpurified reaction products. *J. Med. Chem.* **2014**, *57*, 2845–2850.

(42) (a) Porcari, A. R.; Townsend, L. B. An improved synthesis of the versatile heterocycle, 4-amino-6-bromo-5-cyanopyrrolo[2,3-*d*]-pyrimidine. *Synth. Commun.* **1998**, *28*, 3835–3843. (b) Dang, Q.; Gomez-Galeno, J. E. An efficient synthesis of pyrrolo[2,3-*d*]-pyrimidines via inverse electron demand Diels-Alder reactions of 2-amino-4-cyanopyrroles with 1,3,5-triazines. *J. Org. Chem.* **2002**, *67*, 8703–8705. (c) Taylor, E. C.; Hendess, R. W. Synthesis of pyrrolo[2,3-*d*]pyrimidines. the aglycone of toyocamycin. *J. Am. Chem. Soc.* **1965**, *87*, 1995–2003. (d) Sharma, M.; Bloch, A.; Bobek, M. A practical synthesis of the antibiotic toyocamycin. *Nucleosides Nucleotides* **1993**, *12*, 643–8.

(43) Complex due to F¹⁹-coupling.